



PCCP

Impact of Iodide Ions on the Speciation of Radiolytic Transients in Molten LiCl-KCl Eutectic Salt Mixtures

| | |
|-------------------------------|--|
| Journal: | <i>Physical Chemistry Chemical Physics</i> |
| Manuscript ID | CP-ART-03-2023-001477.R1 |
| Article Type: | Paper |
| Date Submitted by the Author: | 22-May-2023 |
| Complete List of Authors: | Conrad, Jacy K; Idaho National Laboratory, Iwamatsu, Kazuhiro; Brookhaven National Laboratory Department of Chemistry, Woods, Michael; Idaho National Laboratory, Advanced Technology of Molten Salts Gakhar, Ruchi; Idaho National Laboratory, Advanced Technology of Molten Salts Layne, Bobby; Brookhaven National Laboratory, Chemistry Department Cook, Andrew; Brookhaven National Laboratory, Chemistry Department Horne, Gregory; Idaho National Laboratory, Center for Radiation Chemistry Research |
| | |

SCHOLARONE™
Manuscripts

Impact of Iodide Ions on the Speciation of Radiolytic Transients in Molten LiCl-KCl Eutectic Salt Mixtures

Jacy K. Conrad,^{a*} Kazuhiro Iwamatsu,^b Michael E. Woods,^c Ruchi Gakhar,^c Bobby Layne,^b Andrew R. Cook,^b and Gregory P. Horne,^{a*}

^a Center for Radiation Chemistry Research, Idaho National Laboratory, Idaho Falls, ID, P.O. Box 1625, 83415, USA.

^b Department of Chemistry, Brookhaven National Laboratory, Upton, New York, 11973, USA.

^c Advanced Technology of Molten Salts, Idaho National Laboratory, Idaho Falls, ID, P.O. Box 1625, 83415, USA.

*Corresponding authors. E-mail: jacy.conrad@inl.gov and gregory.horne@inl.gov.

ORCID

| | |
|-------------------|---------------------|
| Jacy K. Conrad | 0000-0002-0745-588X |
| Kazuhiro Iwamatsu | 0000-0002-5977-6896 |
| Michael E. Woods | 0000-0001-8685-6026 |
| Ruchi Gakhar | 0000-0002-7103-1256 |
| Bobby Layne | 0000-0002-1225-3596 |
| Andrew R. Cook | 0000-0001-6633-3447 |
| Gregory P. Horne | 0000-0003-0596-0660 |

ABSTRACT

The fate of fission-product iodine is critical for the deployment of next generation molten salt reactor technologies, owing to its volatility and biological impacts if it were to be released into the environment. To date, little is known on how ionizing radiation fields influence the redox chemistry, speciation, and transport of iodine in high temperature molten salts. Here we employ picosecond electron pulse irradiation techniques to elucidate for the first time the impact of iodide ions (I^-) on the speciation and chemical kinetics of the primary radiation-induced transient radicals generated in molten chloride salt mixtures (e_s^- and $Cl_2^{\bullet-}$) as a function of temperature (400–700 °C). In the presence of I^- ions (≥ 1 wt.% KI in LiCl-KCl eutectic), we find that the transient spectrum following the electron pulse is composed of at least three overlapping species: the e_s^- and the $Cl_2^{\bullet-}$ and ICl_2^- radical anions, for which a deconvoluted spectrum of the latter is reported here for the first time in molten salts. This new transient spectrum was consistent with gas phase density functional theory calculations. The lifetime of the e_s^- was unaffected by the addition of I^- ions. The newly observed interhalogen radical anion, ICl_2^- , exhibited a lifetime on the order of microseconds over the investigated temperature range. The associated chemical kinetics indicate that the predominate mechanism of ICl_2^- decay is via reaction with the $Cl_2^{\bullet-}$ radical anion. The iodine containing product of this reaction is expected to be ICl_2^- , which will have implications for the transport of fission-product iodine in MSR technologies.

INTRODUCTION

Nuclear energy is an integral part of the clean energy portfolio needed to minimize anthropogenic climate change. New reactors are required to meet the ever-increasing global energy demand, of which molten salt reactor (MSR) concepts are being championed for their capacity to provide safe, cost-efficient, and sustainable commercial electricity from nuclear fission.^{1,2} However, our fundamental understanding of molten salts in radiation environments is limited,^{3–13} compared to complementary water-cooled reactor technologies.^{14,15} For example, extensive fundamental studies have been done for the radiation-induced fate of fission-product iodine in water-cooled reactor environments,¹⁶ owing to government regulations on the health and safety concerns surrounding the uptake of radioiodine by the thyroid gland if it were to be released into the environment.¹⁷ Additionally, iodine-135 is a precursor to xenon-135, which is a very powerful neutron poison that can drastically impact reactor operations,¹⁸ as evident from the Chernobyl reactor disaster.¹⁹ Consequently, understanding the radiation-induced redox chemistry, speciation, and transport of fission-product iodine in nuclear energy systems is important. That said, the fate of iodine in a MSR is currently unclear, as evidenced by the original Molten Salt Reactor Experiment (MSRE),²⁰ during which up to 70 % of the iodine generated could not be accounted for in the fuel salt or attendant vapor phase. Therefore, to maintain MSR research momentum and accelerate the deployment of new, safe, clean nuclear energy technologies, significant advances are needed to understand the basic and fundamental radiation-induced behavior of fission product iodine in molten salt environments.

The absorption of ionizing radiation (γ) by a molten halide salt ($M^{n+}X_n^-$) leads to the formation of transient excess electrons (e^-) and halide radicals (X^\bullet):^{3–11,13}



These initial radiolytic species can undergo additional chemistry should they escape geminate/non-geminate recombination:



The e^- undergoes successive energy transfer events prior to capture and ultimately solvation (e_s^-)—defined here as a cavity electron coordinated by metal cations (M^{n+})—or reduction of the metal ion component(s) of a given halide salt:^{3–13}

PCCP



On the other hand, the X^\bullet radical rapidly reacts with a neighboring halide anion (X^-) to yield the corresponding dihalogen radical anion ($X_2^{\bullet-}$), which typically undergoes disproportionation:^{3,6,7,13}



and its product X_3^- leads to the equilibrium reaction:



Impurities and other intentional additives, such as transition metal ions, may also act as scavengers for the e_s^- and $X_2^{\bullet-}$ radical anion.¹³ These primary molten salt radiolysis products (e_s^- and $X_2^{\bullet-}$) have been identified in neat molten chloride, bromide, and iodide salts, and the chemical kinetics established for their reactions with several metal ion solutes.^{3,6,7,13} These radiation-induced processes have the capacity to change the corrosion potential of a molten salt and promote the generation of hazardous halide gases and the formation of metal clusters.¹² The impacts of these processes on the performance and longevity of a MSR are currently unknown. Consequently, understanding the basic radiation chemistry of a molten salt is critical for future nuclear energy technologies reliant on this medium.

Under envisioned MSR conditions, for which both fluoride and chloride salt systems have been proposed as reactor coolant and fuel matrix candidates, fission-product iodine can be present as a solute in the bulk salt. Some MSRs are designed to operate with the fuel, and ultimately the fission products, directly dissolved in the molten salt, therefore this situation is not limited to accident scenarios the way it is for water-cooled reactor technologies. Dissolved iodine ions (I^-) have the capacity to act as chemical scavengers of the aforementioned radiolysis products and could yield interhalogen and polyhalide species, for example:



The impacts of these potential interhalogen species (e.g., $XI^{\bullet-}$, XI_2^- , X_2I^- , and XI) on MSR performance and longevity are unknown.

PCCP

With this in mind, and the fact that fission-product iodine is expected to be present as a solute in both the coolant and fuel matrix salts of a MSR, it is necessary to address the impacts of dissolved I^- ions on the basic chemistry of the primary products of molten chloride salt radiolysis. Here, integrated picosecond electron pulse irradiation and transient absorption spectroscopy techniques were employed for the first time to measure the impact of I^- ions (≤ 10 wt.%) on the decay of the e_s^- and $Cl_2^{\bullet-}$ radical anion in lithium chloride-potassium chloride (LiCl-KCl) eutectic salt mixture over a range of temperatures (400–700 °C). Additionally, a combination of Spectro-Kinetic Analysis (*SK-Ana* [21]) software and gas-phase Density Functional Theory (DFT) calculations were employed to evaluate the formation and decay of the new transient iodide chloride radical anion ($ICl^{\bullet-}$).

METHODS

Chemicals. Acetone (≥ 99.5 % purity, ACS reagent), isopropanol (≥ 99.5 % purity, ACS reagent), lithium chloride-potassium chloride eutectic (LiCl-KCl, anhydrous beads, 99.99 % trace metal basis), methanol (MeOH, ≥ 99.9 %), potassium iodide (KI, ≥ 99.99 % purity), and sodium hydroxide (NaOH, 99.99 % trace metals basis) were procured from Millipore-Sigma and used without further purification. Redistilled zinc chloride ($ZnCl_2$) was sourced from Oak Ridge National Laboratory.¹³ Compressed argon (Ar) and nitrous oxide (N_2O) were purchased from Airgas (Radnor, PA, USA) with purities ≥ 99.5 %.

Salt Sample Preparation. Salt mixtures for irradiation were prepared at both Idaho National Laboratory (INL: ≤ 10 wt.% KI in LiCl-KCl eutectic) and Brookhaven National Laboratory (BNL: 0.5–10 wt.% KI in LiCl-KCl eutectic, and 10 wt.% KI + 2 wt.% $ZnCl_2$ in LiCl-KCl eutectic). The compositions (wt.%, mol%, and molarity) for each salt studied at each temperature are summarized in **Table 1**, alongside the electron fractions of each ion in the mixture, as determined from their atomic masses and number of electrons.²²

INL salt mixtures were prepared by mixing the appropriate weighed amounts of solid KI (≤ 10 wt.%) and LiCl-KCl eutectic in a glassy carbon crucible (GAT6, 64 mL Sigradur tapered crucible, HTW, Germany). Masses were recorded to 0.1 mg precision using a Mettler-Toledo balance (Model # TLE204E). The crucible was sequentially cleaned with acetone and isopropanol, dried in a vacuum oven (VWR Symphony, Radnor, PA, USA) at 120 °C for 3 hours, and then left

in an Ar-atmosphere glovebox (VTI, Gloucester, MA, USA) at 600 °C overnight prior to use to remove any residual moisture. The solid salts were then stirred and heated to 500 °C for 6 hours to ensure homogeneity using a box furnace (ThermoScientific, Thermolyne, Model # FB1315M) inside an Ar-atmosphere glovebox. The salt mixtures were then allowed to solidify and cool prior to removal from the crucible, being ground to a powder in an agate mortar and pestle, and then loaded and flame-sealed in modified (extended quartz-borosilicate graded seal stems) 5 × 5 mm Suprasil quartz cuvettes (Spectrocell, Orelan, PA, USA) under vacuum. Flame sealed samples and 1–10 wt.% KI in LiCl-KCl eutectic in sealed vials were shipped to BNL for irradiation and further sample preparation, respectively.

Table 1. Compositions of the KI and LiCl-KCl eutectic salt mixtures and their corresponding electron fractions.²²

| [KI] (wt.%) | Molar Ratio (mol%) | | [KI] (mM) | | | | Electron Fraction (%) | | | |
|----------------|-----------------------|------|--------------|--------|--------|--------|--------------------------|-----------------|-----------------|----------------|
| | LiCl-KCl | KI | 400 °C | 500 °C | 600 °C | 700 °C | I ⁻ | Cl ⁻ | Li ⁺ | K ⁺ |
| 0.054 | 99.98 | 0.02 | 5.410 | 5.242 | 5.074 | 4.906 | 0.04 | 67.34 | 4.34 | 28.29 |
| 0.107 | 99.96 | 0.04 | 10.83 | 10.50 | 10.16 | 9.825 | 0.07 | 67.31 | 4.34 | 28.28 |
| 0.536 | 99.82 | 0.18 | 54.24 | 52.56 | 50.88 | 49.19 | 0.36 | 67.04 | 4.32 | 28.27 |
| 1.072 | 99.64 | 0.36 | 108.7 | 105.34 | 102.0 | 98.58 | 0.73 | 66.71 | 4.30 | 28.25 |
| 5.107 | 98.22 | 1.78 | 526.2 | 509.8 | 493.4 | 477.0 | 3.49 | 64.23 | 4.14 | 28.13 |
| 9.998 | 96.40 | 3.60 | 1050 | 1017 | 984.5 | 951.6 | 6.87 | 61.20 | 3.94 | 27.99 |

BNL salt mixtures were prepared by directly loading the aforementioned vial stocks and weighed mixtures thereof with and without the addition of 2 wt.% ZnCl₂ in 5 × 5 mm Suprasil quartz cuvettes in an Ar-atmosphere glovebox (Mbraun, Garching, Germany). These additional samples were then connected to Swagelok fittings with a sealed quarter turn valve, removed from the Ar-atmosphere glovebox and transferred to a vacuum line, and then flame sealed under vacuum prior to irradiation.

Time-Resolved Electron Pulse Irradiations. The impact of I⁻ ions on the chemical kinetics and speciation of the e_s⁻ and X₂⁻ radical anion in molten LiCl-KCl eutectic salt mixtures was investigated using integrated picosecond electron pulse irradiation and transient absorption spectroscopy techniques at the BNL Laser-Electron Accelerator Facility (LEAF).²³ The above salt mixture samples were loaded into a high-temperature cell holder and heated to the desired temperature (400–700 °C).²⁴ Upon reaching a given temperature, samples were allowed to thermally equilibrate for 10 minutes prior to irradiation to ensure homogeneity. Irradiations

PCCP

comprised of 8.7 MeV electron pulses followed by an anti-colinear xenon-lamp pulse. The BNL LEAF absorption detection system has been previously described in detail.²³ Dosimetry was performed using standard solution²⁵ at the beginning and end of a given day, affording an average dose per pulse of 6–9 Gy water equivalent. Calculated doses were subsequently corrected for the relative density difference between the standard solution and the targeted molten salt sample, assuming the salt densities behaved as an ideal mixture.

Spectro-Kinetic Analysis. Deconvolution of the measured transient absorption spectra was necessary to resolve overlapping radical components. *SK-Ana* software, version 3.4,²¹ was employed for this purpose by using the known spectra for the $\text{Cl}_2^{\cdot-}$ radical anion as an input value in the fit.¹³ *SK-Ana* uses singular value decomposition (SVD) and alternating least squares (ALS) to deconvolute multiple species' spectra which are superimposed in the observed wavelength range and optimize the kinetics and spectral shapes of the components to achieve a best fit. Following deconvolution, measured product decay kinetics were fit as near to their absorption maxima as possible. The decay of the e_s^- was studied at 671 nm, the decay of the $\text{Cl}_2^{\cdot-}$ radical anion was studied at 340 nm, and the decay of the newly measured $\text{ICl}^{\cdot-}$ radical anion was observed at 400 nm. The kinetics for the e_s^- were fit using a single exponential decay to yield pseudo-first-order rate coefficients (k') for each concentration of KI. The decays of the $\text{Cl}_2^{\cdot-}$ and $\text{ICl}^{\cdot-}$ radical anions were fit using a second-order decay function to yield k/ϵ values ($\text{cm}\cdot\text{s}^{-1}$), where ϵ is the unknown extinction coefficient value of the transient species in the molten chloride salt at a given wavelength ($\text{M}^{-1}\cdot\text{cm}^{-1}$). Oversampled raw-data were boxcar smoothed in the scope to enhance signal:noise without loss of required time-resolution. Quoted errors are a combination of the measurement precision, uncertainty in the fitted parameters, and sample concentration errors.

Computational Methods. Geometry optimizations and frequency calculations were performed for $\text{Cl}_2^{\cdot-}$, $\text{ICl}^{\cdot-}$, and $\text{I}_2^{\cdot-}$ radical anions using DFT to determine their lowest energy configurations. *Gaussian 16* software²⁶ was used to run calculations for the $\text{X}_2^{\cdot-}$ radical anion species in the gas phase using the B3LYP/6-311++G(d,p) level of theory for the chlorine atom, and the Def2TZVP effective core potential (ECP) basis set for the iodine atom.^{27–29} All optimized geometries were found to be minima on the potential energy surface using harmonic vibrational frequency analysis at the same level of theory. The minimum energy structures were analyzed using time-dependent density functional theory (TD-DFT) to predict electronic absorption spectra using the same level of theory.

RESULTS AND DISCUSSION

Spectral Deconvolutions. Dose-normalized transient spectra for the irradiation of neat LiCl-KCl eutectic and 10 wt.% KI in LiCl-KCl eutectic as a function of time at 400 °C are shown in **Fig. 1A** and **1B**, respectively.

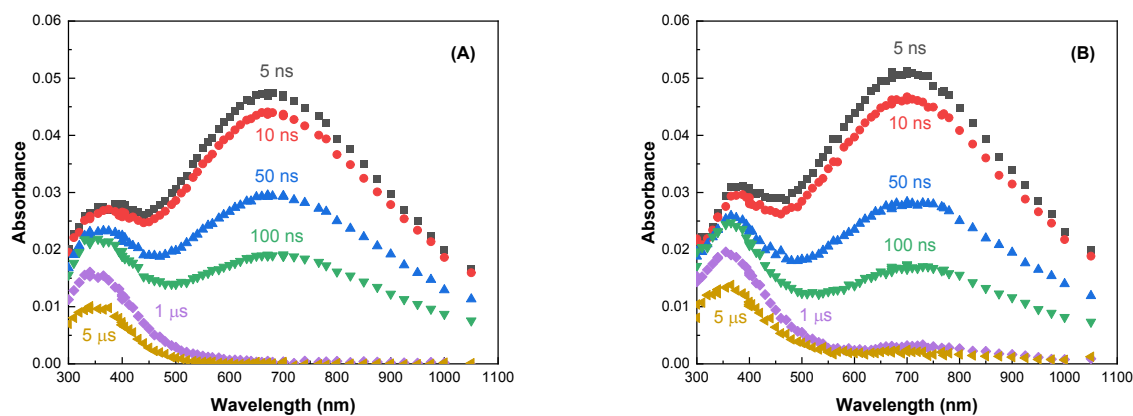


Fig. 1. Transient absorption spectra from the electron pulse irradiation of neat LiCl-KCl eutectic (**A**) and 10 wt.% KI in LiCl-KCl eutectic (**B**) at 400 °C for: 5 ns (■), 10 ns (●), 50 ns (▲), 100 ns (▼), 1 μs (◆), and 5 μs (◄) normalized by the absorbed dose.

Additional transient spectra for the lower concentrations of KI in LiCl-KCl eutectic shown in **Table 1** are given in the **Supplementary Information (SI)**. There are two distinct absorption bands common to both molten salt systems. Both bands decay as a function of time, albeit the one at higher wavelengths is shorter lived. From previous work on the irradiation of neat LiCl-KCl eutectic at 400 °C:¹³ the short-lived (< 1 μs) species with the broad absorption band in the visible and near-infrared (nIR) is attributed to the e_s^- in **Fig. 1A** and **1B**. The e_s^- peak maximum appears to be shifted to longer wavelength when 10 wt.% KI is present. When 10 wt.% of KI is added to LiCl-KCl, the molar ratio of $Li^+ : K^+$ changes from 58:42 (neat LiCl-KCl) to 56:44. Hagiwara *et al.* reported peak maxima shifts from 515 to 790 nm for 0 to 50 mol% of K^+ in LiCl-KCl mixtures at 600 °C. According to their work, a 2 mol% difference should yield an ~10 nm shift in the e_s^- peak maximum.⁸ The 20–30 nm shift observed in **Fig. 1A** and **1B** can be attributed to these effects, plus the contribution of other absorbing species from I^- , such as the mixed halide radical anion ICl_2^- , to be discussed in more detail later. The second, longer-lived (> 20 μs) species, with a narrower absorption band in the ultra-violet (UV), is attributed to the Cl_2^- radical anion in **Fig. 1A**. In the

PCCP

presence of ≥ 1 wt.% KI there is at least one additional species absorbing around 400 nm, most likely attributed to a mixture of one or more $X_2^{\bullet-}$ radical anions, as seen in **Fig. 1B** and **SI Fig. S1**.

The initial mixture of $X_2^{\bullet-}$ radical anions after the pulse could potentially comprise $Cl_2^{\bullet-}$, $ICl^{\bullet-}$, and $I_2^{\bullet-}$, arising from a combination of direct and indirect radiation effects on both halide anions:



When we compare the electron fractions listed in **Table 1**, it is clear that Cl^- ions are much more likely to interact directly with radiation via **Eq. 9** when compared to the I^- ions. In addition, because there are significantly more Cl^- ions in the mixtures (see **Table 1**), indirect radiation effects from secondary reactions are far more likely to proceed via interaction with Cl^- ions rather than I^- ions. Consequently, the majority of the radiation energy will be deposited into the Cl^- ion component of a given salt mixture in **Table 1**. Therefore, there will be a significantly greater initial yield of Cl^{\bullet} radicals vs. I^{\bullet} radicals in the investigated salt mixtures, and **Eq. 10** is expected to dominate. The formation of the $I_2^{\bullet-}$ radical anion (**Eq. 13**) is therefore unlikely given the low direct effect yield of I^{\bullet} radicals and their likelihood of being subsequently scavenged by the more abundant Cl^- ions (**Eq. 12**). This indicates that the second deconvoluted species in the UV for ≥ 1 wt.% KI is the $ICl^{\bullet-}$ radical anion, formed by a combination of **Eq. 11** and **12**, the respective contributions of which are dictated by the electron fractions of the ions and their probability of ionization in the salt mixtures. Therefore, one can conclude that the transients observed in the UV region of **Fig. 1B** and **SI Fig. S1** are a mixture of $Cl_2^{\bullet-}$ and $ICl^{\bullet-}$ radical anions, where the $Cl_2^{\bullet-}$ radical anion is the dominant species. A summary of the observed species in the irradiated KI in LiCl-KCl eutectic mixtures is given in **Table 2**.

Table 2. Summary of transient radicals observed in irradiated KI in LiCl-KCl eutectic mixtures.

| Species | $\sim\lambda_{\max}$ (nm) | Lifetime (μs) |
|--------------------------|---------------------------|----------------------------|
| e_s^- | 700 | < 1 |
| $\text{Cl}_2^{\bullet-}$ | 340 | > 20 |
| $\text{ICl}^{\bullet-}$ | 400 and 710 | > 20 |

The deconvoluted spectra of the above species are given in **Fig. 2A** and **2B** for the first microsecond after the electron pulse, normalized to a maximum absorption of 1.0. The rotational ambiguity plots for these fits are shown in **SI Fig S2**. Although an absorption spectrum for the $\text{ICl}^{\bullet-}$ radical anion has not been measured previously, transient spectra for the $\text{Cl}_2^{\bullet-}$ and $\text{I}_2^{\bullet-}$ radical anions have been reported in a variety of media, including high temperature molten salts.^{3,6,7,13} These $\text{X}_2^{\bullet-}$ radical anion spectra, and that reported for the e_s^- in molten salts,^{4,7,13} were used to compare with the *SK-Ana* deconvolution of the multiple overlaid components in **Fig. 1A** and **1B**. The deconvoluted spectra for neat molten LiCl-KCl eutectic (**Fig. 2A**) agree with previous findings,¹³ i.e., that there are two major absorbing components, the e_s^- and the $\text{Cl}_2^{\bullet-}$ radical anion with $\lambda_{\max} = 700$ and 340 nm, respectively. Interestingly, deconvolution of the 10 wt.% KI in LiCl-KCl system (**Fig. 2B**) shows a mixture of the e_s^- , the $\text{Cl}_2^{\bullet-}$ radical anion, and a single other $\text{X}_2^{\bullet-}$ radical anion species in the UV region ($\lambda_{\max} = 400$ nm), the spectrum for which is clearly distinguishable from that of the $\text{Cl}_2^{\bullet-}$ radical anion at KI concentrations of ≥ 1 wt.%. Deconvoluted spectra for the other KI concentrations are given in **SI Fig. S3**. As discussed above, we attribute this second component to the $\text{ICl}^{\bullet-}$ radical anion. Note, the deconvoluted spectrum for the e_s^- in **Fig. 2B** appears to be artificially distorted at its peak by the underlying $\text{ICl}^{\bullet-}$ radical anion spectrum, as compared to **Fig. 2A**. Scavenger studies, discussed later, were performed to evaluate this.

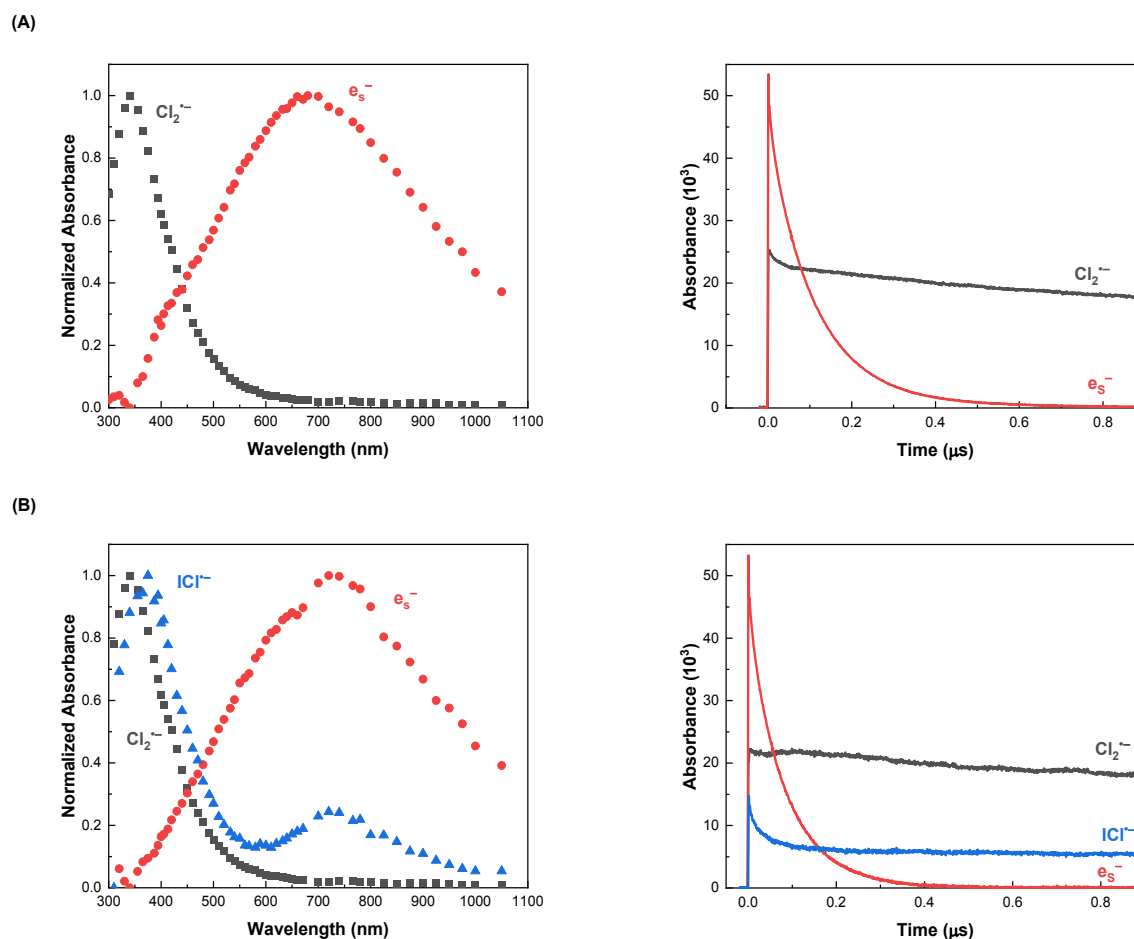


Fig. 2. Normalized spectra and kinetics from *SK-Ana* deconvolution of the electron pulse irradiation of neat LiCl-KCl eutectic (A) and 10 wt.% KI in LiCl-KCl eutectic (B) at 400 °C up to 1 μs.

Assignment of the second UV absorbing species to the $\text{ICl}^{\cdot-}$ radical anion is supported by the deconvoluted spectrum's lack of similarity to the reported spectrum for the $\text{I}_2^{\cdot-}$ radical anion in neat molten KI at 700 °C, where its absorption maximum is found at ~450 nm.⁶ This is a significant shift from the deconvoluted spectrum in **Fig. 2B** and **SI Fig. S3**. Moreover, Hagiwara *et al.* reported no peak shift for the $\text{Cl}_2^{\cdot-}$ radical anion spectrum as a function of temperature, therefore, we should not expect that the $\text{I}_2^{\cdot-}$ radical anion spectrum would be significantly changed at 400 °C.

Gas phase TD-DFT calculations for all three possible transient $\text{X}_2^{\cdot-}$ radical anions ($\text{Cl}_2^{\cdot-}$, $\text{ICl}^{\cdot-}$, and $\text{I}_2^{\cdot-}$), shown in **Fig. 3**, further support this assignment. Although these are gas-phase calculations, the maximum absorbance of the $\text{Cl}_2^{\cdot-}$ radical anion agrees extremely well with the experimental value in molten chloride salts.^{6,13} The theoretical spectrum for the $\text{I}_2^{\cdot-}$ radical anion is less close to that observed experimentally as its wavelength maximum is shifted about 100 nm

to the red, and its second peak at ~ 750 nm is not predicted, potentially suggesting a charge transfer band. A subject for a future investigation. With these observations in mind, the computational spectra should be used as a guideline only. The calculated spectrum for the ICl_2^- radical anion puts its maxima between the Cl_2^- and the I_2^- radical anion spectra and suggests significant overlap with that of the Cl_2^- radical anion spectrum, as predicted by *SK-Ana* in **Fig. 2B**, further justifying our assignment.

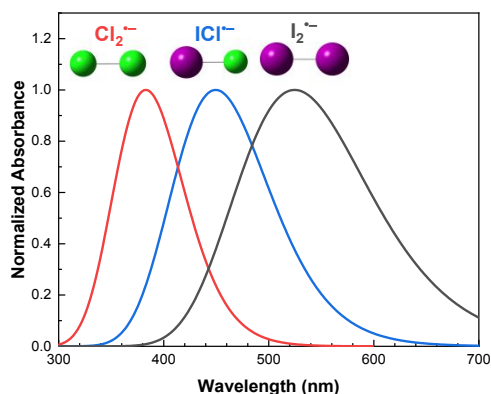


Fig. 3. Normalized theoretical gas phase absorption spectra for Cl_2^- , ICl^- , and I_2^- radical anions, as calculated by TD-DFT.

As demonstrated previously,¹³ when ZnCl_2 is added to molten LiCl-KCl eutectic, the divalent zinc cation (Zn^{2+}) acts as an electron scavenger:



effectively removing the e_s^- , and likely its precursor (e^-), from the resulting transient absorption spectrum and increasing the initial yield of the Cl_2^- radical anion by inhibiting the following reactions:¹³



This scavenging effect is shown in **Fig. 4A** for 5 ns after the electron pulse for 10 wt.% KI in LiCl-KCl eutectic at 400°C with and without the addition of 2 wt.% ZnCl_2 . The corresponding *SK-Ana* deconvolution of the ZnCl_2 containing salt mixture is shown in **Fig. 4B**, again showing the two distinct transient species. These species were again assigned to the Cl_2^- and ICl^- radical anions and are consistent with those observed in the absence of ZnCl_2 (**Fig. 2B**). The kinetics associated

with these deconvoluted spectra are shown in **SI Fig. S4**. These deconvolutions lend further credence to the fact that the spectrum of the ICl^- radical anion has two primary absorption peaks, like those seen for the Br_2^- and I_2^- radical anions.⁶ This second absorption peak (~ 575 to 1100 nm) is likely the cause of the more intense e_s^- band in **Fig. 1B**, relative to the neat LiCl-KCl eutectic mixture absorption band in **Fig. 1A**.

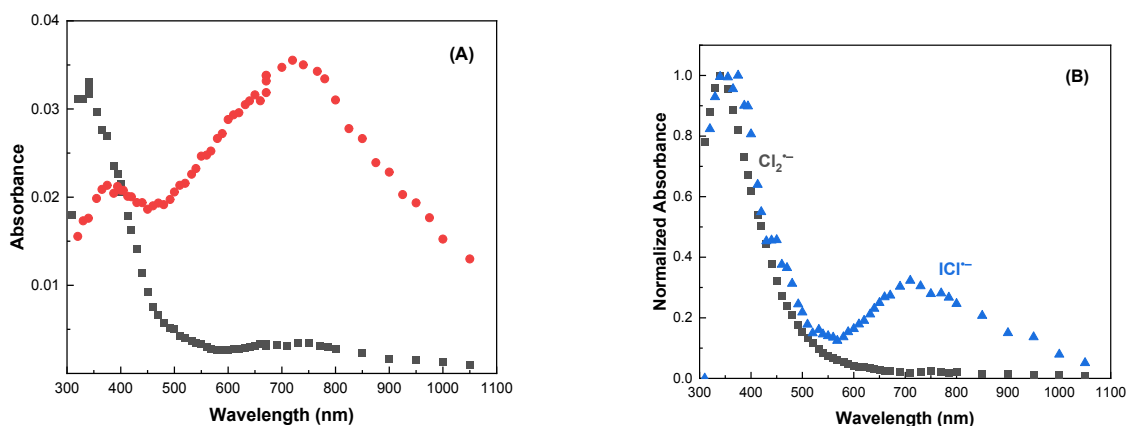


Fig. 4. Transient absorption spectra 5 ns after electron pulse irradiation of 10 wt.% KI in LiCl-KCl eutectic without (●) and with (■) the addition of ~ 2 wt.% ZnCl_2 at 400 °C (A). Normalized spectra from *SK-Ana* deconvolution of the ZnCl_2 containing salt mixture at 400 °C (B).

PCCP

Kinetics of Transient Decays. The rate of decay for the e_s^- was fitted by a single exponential function over the first 350–600 ns after the electron pulse to yield pseudo-first-order rate coefficients for each concentration of KI in LiCl-KCl eutectic over the range of temperatures (400–700 °C), summarized in **SI Table S1**. These exponential decay fits over the initial 500 ns after the electron pulse are shown in **SI Fig. S5** alongside the corresponding natural logarithm plots, showing the timescale for which the pseudo-first-order behavior is observable. The decay rate of the e_s^- in molten salts is known to be dictated by impurities in the base salt, such as multivalent metal ions and protons from residual moisture.¹³ Here, there was no trend observed in the calculated pseudo-first order rate coefficients (**Table S1**) as a function of the KI concentration, indicating that the I^- ions, their associated radiolysis products, and the additional impurities in the KI salt do not react significantly with the e_s^- relative to the base LiCl-KCl eutectic salt's impurities. In all cases, the natural logarithm of the pseudo-first-order decay rate of the e_s^- increased linearly with increasing inverse temperature (**SI Fig. S6**).

Of more interest were the fitted second-order decays for the $Cl_2^{\bullet-}$ and $ICl^{\bullet-}$ radical anions after the electron pulse. At wavelengths from 300–600 nm, the observed absorbance decay trace is a mixture of the two radical anion species, according to their deconvoluted spectra in **Fig. 2B**. Consequently, the absorbance vs. time plots within this wavelength range are the sum of the contributions from the $Cl_2^{\bullet-}$ and $ICl^{\bullet-}$ radical anions, which complicates the deconvolution of their respective decay rates, especially in the absence of their molar extinction coefficients. However, isolation of the $ICl^{\bullet-}$ radical anion's decay kinetics was achieved by using its absorbance at 671 nm at times $> 1 \mu s$, when the e_s^- had completely decayed (**Fig. 1A**). The second-order absorbance decays were plotted as a function of time at $t > 1 \mu s$ and fit to yield k/ϵ_{671nm} values ($cm \cdot s^{-1}$), where ϵ_{671nm} is the unknown extinction coefficient of the $ICl^{\bullet-}$ radical anion at 671 nm in the given salt mixture at the given temperature. The fitted absorbance for the $ICl^{\bullet-}$ radical decay for 10 wt.% KI in the LiCl-KCl eutectic at times $> 1 \mu s$ at 671 nm are shown in **Fig. 5**.

PCCP

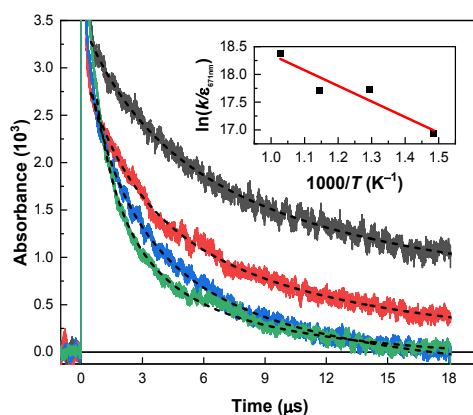


Fig. 5. The fitted absorbance for the $\text{ICl}_2^{\bullet-}$ radical anion decay at $t > 1 \mu\text{s}$ at 671 nm after the electron pulse irradiation of 10 wt.% KI in LiCl-KCl eutectic at 400 (—), 500 (—), 600 (—), and 700 (—) °C. Inset: associated Arrhenius plot.

By plotting the natural logarithm of the $k/\epsilon_{671\text{nm}}$ values against inverse temperature, linear Arrhenius plots were obtained for all concentrations of KI (SI Fig. S7). The 10 wt.% KI in LiCl-KCl eutectic Arrhenius plot is given in the inset of Fig. 5, demonstrating that the temperature dependence of the $\text{ICl}_2^{\bullet-}$ radical anion decay is proportional to $\ln(k/\epsilon_{671\text{nm}})$. The Arrhenius plot is linear over the given temperature range, affording an activation energy of $E_a = 23.4 \pm 5.7 \text{ kJ mol}^{-1}$ and pre-exponential factor of $A/\epsilon_{671\text{nm}} = (1.6 \pm 1.3) \times 10^9 \text{ cm} \cdot \text{s}^{-1}$ for the disproportionation of the $\text{ICl}_2^{\bullet-}$ radical anion. This activation energy is similar to that observed for the disproportionation of the $\text{Cl}_2^{\bullet-}$ radical cation in LiCl-KCl eutectic ($24\text{--}26 \text{ kJ mol}^{-1}$).¹³ Similarly, the combined decay of the $\text{Cl}_2^{\bullet-}$ and $\text{ICl}_2^{\bullet-}$ radical anions can be approximately fit by a single second-order function and the equivalent $\ln(\sum k/\epsilon)$ vs. inverse temperature plots are shown in SI Fig. S8–S9 for 340 nm and 400 nm, again showing an increase in the decay rate with temperature.

It should be noted that Iwamatsu *et al.* identified a trend in the observed second-order decay of the $\text{Cl}_2^{\bullet-}$ radical anion with absorbed dose in the neat LiCl-KCl eutectic at 400 °C.¹³ As the dose delivered by the electron pulse was increased, the observed rate of the $\text{Cl}_2^{\bullet-}$ radical anion decay decreased. The change in $\text{Cl}_2^{\bullet-}$ radical anion decay with dose rate was attributed to salt impurities (S) reacting with the e_s^- and subsequently acting as $\text{Cl}_2^{\bullet-}$ radical anion scavengers:



These reactions have a non-negligible contribution at low doses per electron pulse, and doses of $> 70 \text{ Gy pulse}^{-1}$ are required to entirely out compete them with the second-order $\text{Cl}_2^{\bullet-}$ radical anion

disproportionation process, owing to the greater initial yield of the $\text{Cl}_2^{\cdot-}$ radical anion per pulse. Comparison of our derived $\text{Cl}_2^{\cdot-}$ radical anion decay rates for the neat LiCl-KCl eutectic with those from previous studies (SI Fig. S10) show that our values are in good agreement with those reported within the low dose rate regime. Consequently, we also expected some portion of our $\text{ICl}^{\cdot-}$ radical anion decay rates to be composed of impurity driven reactions.

Transient Decay Mechanisms. Plots of $1/\text{absorbance}$ vs. time can be used to provide additional insights on the $\text{ICl}^{\cdot-}$ radical anion decay mechanism. It is known from a previous study on the decay of the $\text{Cl}_2^{\cdot-}$ radical anion in molten neat LiCl-KCl eutectic that this species is primarily consumed via its disproportionation reaction, resulting in a second-order decay, which gives a linear inverse absorbance plot.¹³ As discussed above, impurities present in the salt mixtures can act as $\text{Cl}_2^{\cdot-}$ scavengers (Eq. 17 and 18) and tend to cause slight deviation from linearity by curving downwards,¹³ as shown in Fig. 6A for the neat LiCl-KCl eutectic at 340 nm.

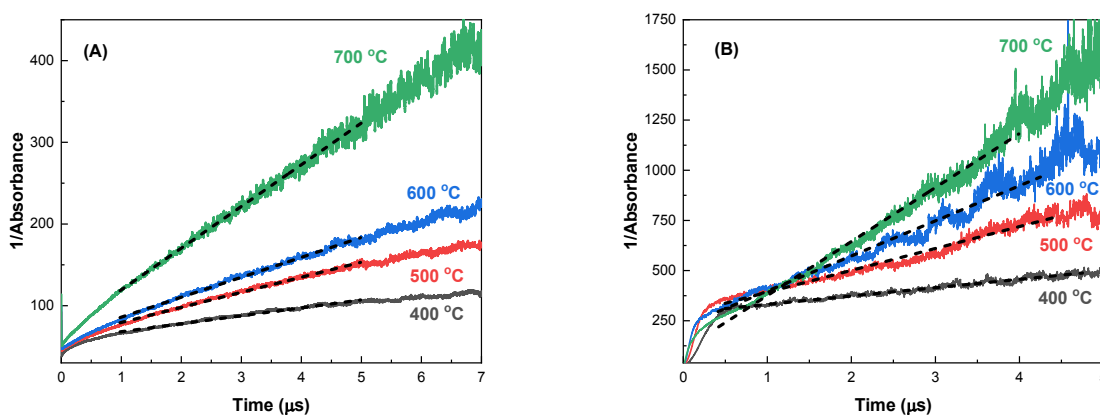


Fig. 6. The fitted inverse absorbance after the electron pulse irradiation of neat LiCl-KCl eutectic at 340 nm (A) and 10 wt.% KI in LiCl-KCl eutectic at 671 nm (B) at 400 (—), 500 (—), 600 (—), and 700 (—) °C.

The $1/\text{absorbance}$ plot for 10 wt.% KI in LiCl-KCl eutectic at 671 nm is shown in Fig. 6B, where at $t > 1 \mu\text{s}$ the entire absorbance corresponds to the $\text{ICl}^{\cdot-}$ radical anion. These plots are also linear, indicating that the primary decay mechanism for $\text{ICl}^{\cdot-}$ is also second order, and likely corresponds to its reaction with the $\text{Cl}_2^{\cdot-}$ radical anion to form $\text{ICl}_2^{\cdot-}$ (Eq. 7). For molten salts containing KI, the inverse absorbance plots at 340 nm and 400 nm deviate from linearity by curving upwards (see SI Fig. S11), likely due to a superposition of the two second-order decay reactions of the $\text{Cl}_2^{\cdot-}$ and $\text{ICl}^{\cdot-}$ radical anions (Eq. 4 and 7) since both species are absorbing at these wavelengths, as shown in Fig. 2B.

CONCLUSIONS

The addition of I^- ions to molten LiCl-KCl eutectic has been found to alter the fundamental radiation chemistry of the system through the formation of a second, transient dihalide radical anion, attributed to $ICl_2^{\bullet-}$. This new species exhibits two main absorption peaks, the first in the UV (~ 380 nm), which overlaps with the $Cl_2^{\bullet-}$ radical anion spectrum, and the second in the visible (~ 710 nm), which becomes apparent after the decay of the e_s^- absorption at μs timescales.

With the KI concentrations (≤ 10 wt.%) and dose rates (6–9 Gy pulse⁻¹ water equivalent) used here, the $ICl_2^{\bullet-}$ radical anion is expected to be predominantly formed by the scavenging of Cl^{\bullet} radicals by I^- ions, and ultimately consumed by its disproportionation reaction with the $Cl_2^{\bullet-}$ radical anion ($E_a = 23.4 \pm 5.7$ kJ mol⁻¹). The iodine containing product of the $ICl_2^{\bullet-}$ disproportionation reaction is expected to be ICl_2^- , analogous to Cl_2^- , thereby providing a potential pathway for the formation of volatile interhalogen species, such as ICl.

These radiation-induced changes in I^- ion speciation likely have significant implications for the transport and accumulation of fission-product iodine in MSR environments. Consequently, they require further study to support the safe development, deployment, and long-term maintenance of promising MSR technologies.

CONFLICTS OF INTEREST

There are no conflicts to declare.

ASSOCIATED CONTENT

Supplementary Information for spectra, deconvolutions, chemical kinetics and Arrhenius plots for other KI concentrations.

AUTHOR INFORMATION

Corresponding Authors

Jacy K. Conrad – Center for Radiation Chemistry Research, Idaho National Laboratory, 1955 N. Fremont Ave., Idaho Falls, 83415, USA; orcid.org/0000-0002-0745-588X; E-mail: jacy.conrad@inl.gov.

Gregory P. Horne – Center for Radiation Chemistry Research, Idaho National Laboratory, 1955 N. Fremont Ave., Idaho Falls, 83415, USA; orcid.org/0000-0003-0596-0660; E-mail: gregory.horne@inl.gov.

ACKNOWLEDGEMENTS

This work was supported by the U.S. Department of Energy (US-DOE), Office of Science, Basic Energy Sciences through the Chemical and Materials Sciences to Advance Clean Energy Technologies and Low-Carbon Manufacturing initiative under contract DE-AC07-05ID14517 and DE-SC0012704 at INL and BNL, respectively. Cook, Layne, and electron pulse irradiation experiments at the LEAF of the BNL Accelerator Center for Energy Research were supported by the US-DOE Office of Basic Energy Sciences, Division of Chemical Sciences, Geosciences, and Biosciences under contract DE-SC0012704. This research made use of Idaho National Laboratory computing resources which are supported by the Office of Nuclear Energy of the U.S. Department of Energy and the Nuclear Science User Facilities under Contract No. DE-AC07-05ID14517. The authors would like to thank Professor Pascal Pernot for his assistance in using the *SK-Ana* software.

REFERENCES

- (1) Ignatiev, J.L. Kloosterman, L. Luzzi, E. Merle-Lucotte, J. Uhlř, R. Yoshioka, and D. Zhimin, The molten salt reactor (MSR) in generation IV: Overview and perspectives. *Prog. Nucl. Energy* **2014**, *77*, 308.
- (2) C.W. Forsberg, Market Basis for Salt-Cooled Reactors: Dispatchable Heat, Hydrogen, and Electricity with Assured Peak Power Capacity. *Nucl. Technol.* **2020**, *206 (11)*, 1659.
- (3) I.E. Makarov, T.N. Zhukova, and A.K. Pikaev, Transient species in radiolysis of melted alkali metal halides. *Rad. Effects*, **1974**, *22*, 71.
- (4) I.E. Makarov, T.N. Zhukova, and A.K. Pikaev, Reactivity of solvated electrons in irradiated melts of alkali halide compounds. *Doklady Akademii Nauk SSSR*, **1975**, *225 (5)*, 1103.
- (5) A.K. Pikaev, B.G. Ershov, and I.E., Makarov, Influence of the Nature of a Matrix on the Reactivity of Electrons in Irradiated Systems. *J. Phys. Chem.* **1975**, *79*, 3025.
- (6) I.E. Makarov, T.N. Zhukova, A.K. Pikaev, and V.I. Spistyn, Oxidizing agents produced by radiolysis of alkali-metal halide melts. *Bulletin of the Academy of Science USSR, Division of Chemical Science (English Translation)*, **1982**, *31(4)*, 662.
- (7) A.K. Pikaev, I.E. Makarov, and T.N. Zhukova, Solvated electron in irradiated melts of alkaline halides. *Rad. Phys. Chem.* **1982**, *19 (5)*, 377.

PCCP

- (8) H. Hagiwara, S. Sawamura, T. Sumiyoshi, and M. Katayama, Pulse radiolysis study of transient species in LiCl-KCl melt. *Rad. Phys. Chem.* **1987**, *30* (2), 141.
- (9) S. Sawamura, J. L. Gebicki, J. Mayer, and J. Kroh, Pulse radiolysis of LiBr-KBr melts. Optical transient absorption spectra. *Rad. Phys. Chem.* **1990**, *36* (2), 133.
- (10) R. Akiyama, M. Kitaichi, T. Fujiwara, and S. Sawamura, Short Lived Species Produced in Pulse Irradiated Melts of LiF-KF and LiF-NaF-KF Eutectic Mixtures. *J. Nucl. Sci. Technol.* **1994**, *31*, 250.
- (11) W.C. Phillips, R. Gakhar, G.P. Horne, B. Layne, K. Iwamatsu, A. Ramos-Ballesteros, M.R. Shaltry, J.A. LaVerne, S.M. Pimblott, and J.F. Wishart, Design and performance of high-temperature furnace and cell holder for in situ spectroscopic, electrochemical, and radiolytic investigations of molten salts. *AIP Rev. Sci. Instr.* **2020**, *91* (8), 083105.
- (12) E.T. Dias, S.K. Gill, Y. Liu, P. Halstenberg, S. Dai, J. Huang, J. Mausz, R. Gakhar, W.C. Phillips, S. Mahurin, S.M. Pimblott, J.F. Wishart, and A.I. Frenkel, Radiation-Assisted Formation of Metal Nanoparticles in Molten Salts. *J. Phys. Chem. Lett.* **2021**, *12*, 157.
- (13) K. Iwamatsu, G.P. Horne, R. Gakhar, P. Halstenberg, B. Layne, S.M. Pimblott, and J.F. Wishart, Radiation-Induced Reaction Kinetics of Zn^{2+} with e_s^- and Cl_2^- in Molten LiCl-KCl Eutectic at 400–600 °C. *Phys. Chem. Chem. Phys.* **2022**, *24*, 25088.
- (14) B.C. Garrett, D.A. Dixon, D.M. Camaioni, D.M. Chipman, M.A. Johnson, C.D. Jonah, G.A. Kimmel, J.H. Miller, T.N. Rescigno, P.J. Rossky, S.S. Xantheas, S.D. Colson, A.H. Laufer, D. Ray, P.F. Barbara, D.M. Bartels, K.H. Becker, K.H. Bowen, S.E. Bradforth, I. Carmichael, J.V. Coe, L.R. Corrales, J.P. Cowin, M. Dupuis, K.B. Eisenthal, J.A. Franz, M.S. Gutowski, K.D. Jordan, B.D. Kay, J.A. LaVerne, S.V. Lymar, T.E. Madey, C.W. McCurdy, D. Meisel, S. Mukamel, A.R. Nilsson, T.M. Orlando, N.G. Petrik, S.M. Pimblott, J.R. Rustad, G.K. Schenter, S.J. Singer, A. Tokmakoff, L.-S. Wang, and T.S. Zwier, Role of Water in Electron-Initiated Processes and Radical Chemistry: Issues and Scientific Advances. *Chem. Rev.*, **2005**, *105* (1), 355.
- (15) A.J. Elliot and D.M. Bartels, The Reaction Set, Rate Constants and G-Values for the Simulation of the Radiolysis of Light Water Over the Range 20° to 350° C Based on Information Available in 2008. AECL Nuclear Platform Research and Development – Report 153-127160-450-001.
- (16) G. Baston, S. Dickinson, H. Roebuck, and H.E. Sims, Radiation chemistry of aqueous iodine at low concentrations. *Rad. Phys. Chem.*, **2021**, *180*, 109099.
- (17) D. Williams, A. Pinchera, A. Karaoglou, and K.H. Chadwick, Thyroid Cancer in Children living near Chernobyl. Commission of the European Communities, EUR-15248, **1993**.
- (18) W.M. Stacey, Nuclear Reactor Physics, Second Edition, WILEY-VCH Verlag GmbH & Co. KGaA, Weinheim, Germany, **2007**.
- (19) M.V. Malko, The Chernobyl Reactor: Design Features and Reasons for Accident in Recent Research Activities About the Chernobyl NPP Accident in Belarus, Ukraine and Russia, pp 11-27. T. Imanaka (Ed.), Research Reactor Institute, Kyoto University, **2002**.

- (20) E.L. Compere, S.S. Kirslis, E.G. Bohlmann, F.F. Blankenship, and W.R. Grimes, Fission product behavior in the Molten Salt Reactor Experiment. ORNL-4865, **1975**.
- (21) P. Pernot, SK-Ana: Analysis of Spectro-Kinetic Data (Version 3.4), **2018**, <https://doi.org/10.5281/zenodo.1064370>, last accessed on 12/08/2022.
- (22) G.J. Janz, C.B. Allen, N.P. Bansal, R.M. Murphy, and R.P.T. Tomkins, Physical Properties Data Compilations Relevant to Energy Storage. II. Molten Salts: Data on Single and Multi-Component Salt Systems (NSRDS-NBS 61, Part II, U.S. Government Printing Office, Washington, 1979).
- (23) J.F. Wishart, A.R. Cook, and J.R. Miller, The LEAF picosecond pulse radiolysis facility at Brookhaven National Laboratory. *Rev. Sci. Instrum.* **2004**, *75* (11), 4359.
- (24) W.C. Phillips, R. Gakhar, G.P. Horne, B. Layne, K. Iwamatsu, A. Ramos-Ballesteros, M.R. Shaltry, J.A. LaVerne, S.M. Pimblott, and J.F. Wishart, *Rev. Sci. Instrum.*, **2020**, *91* (8), 083105.
- (25) A.R. Cook, M.J. Bird, S. Asaoka, and J.R. Miller, Rapid “Step Capture” of Holes in Chloroform during Pulse Radiolysis. *J. Phys. Chem. A* **2013**, *117* (33), 7712.
- (26) M.J. Frisch, G.W. Trucks, H.B. Schlegel, G.E. Scuseria, M.A. Robb, J.R. Cheeseman, G. Scalmani, V. Barone, G.A. Petersson, H. Nakatsuji, X. Li, M. Caricato, A.V. Marenich, J. Bloino, B.G. Janesko, R. Gomperts, B. Mennucci, H.P. Hratchian, J.V. Ortiz, A.F. Izmaylov, J.L. Sonnenberg, D. Williams-Young, F. Ding, F. Lipparini, F. Egidi, J. Goings, B. Peng, A. Petrone, T. Henderson, D. Ranasinghe, V.G. Zakrzewski, J. Gao, N. Rega, G. Zheng, W. Liang, M. Hada, M. Ehara, K. Toyota, R. Fukuda, J. Hasegawa, M. Ishida, T. Nakajima, Y. Honda, O. Kitao, H. Nakai, T. Vreven, K. Throssell, J.A. Montgomery, J.E. Peralta, F. Ogliaro, M.J. Bearpark, J.J. Heyd, E.N. Brothers, K.N. Kudin, V.N. Staroverov, T.A. Keith, R. Kobayashi, J. Normand, K. Raghavachari, A.P. Rendell, J.C. Burant, S.S. Iyengar, J. Tomasi, M. Cossi, J.M. Millam, M. Klene, C. Adamo, R. Cammi, J.W. Ochterski, R.L. Martin, K. Morokuma, O. Farkas, J.B. Foresman, and D.J. Fox, Gaussian 16, Revision C.01; Gaussian Inc.: Wallingford, CT, **2016**.
- (27) A.D. Becke, Density-Functional Thermochemistry 3. The Role of Exact Exchange. *J. Chem. Phys.*, **1993**, *98* (7), 5648.
- (28) C.T. Lee, W.T. Yang, and R.G. Parr, Development of the Colle-Salvetti Correlation Energy Formula into a Functional of the Electron Density. *Physical Review B*, **1988**, *37* (2), 785.
- (29) C.K. Kim, S.H. Yoon, J. Wong, and C.K. Kim, Examination of Gaussian-Type Basis Sets on Alkali Metal Halides. *Bull. Korean Chem. Soc.*, **2006**, *27* (8), 1219.